Theor Chem Acc (2007) 118:211–218
DOI 10.1007/s00214-007-0272-z

REGULAR ARTICLE

Potential energy functions for an intramolecular proton transfer reaction in the ground and excited state

Alessandro Cembran · Jiali Gao

Received: 3 December 2006 / Accepted: 22 February 2007 / Published online: 28 March 2007

Abstract We describe the development of empirical potential functions for the study of the excited state intramolecular proton transfer reaction in 1-(trifuloroacetylamino)-naphtaquinone (TFNQ). The potential is a combination of the standard CHARMM27 force field for the backbone structure of TFNQ and an empirical valence bond formalism for the proton transfer reaction. The latter is parameterized to reproduce the potential energies both in the ground and the excited state, determined at the CASPT2 level of theory. Parameters describing intermolecular interactions are fitted to reproduce molecular dipole moments computed at the CASSCF level of theory and to reproduce ab initio hydrogen bonding energies and geometries for TFNQ-water bimolecular complexes. The utility of this potential energy function was examined by computing the potentials of mean force for the proton transfer reactions in the gas phase and in water, in both electronic states. The ground state PMF exhibits little solvent effects, whereas computed potential of mean force shows a solvent stabilization of 2.5 kcal mol^{-1} in the product state region, suggesting proton transfer is more pronounced in polar solvents, consistent with experimental findings.

Electronic supplementary material The online version of this article (doi:10.1007/s00214-007-0272-z) contains supplementary material, which is available to authorized users.

Contribution to the Fernando Bernardi Memorial Issue.

A. Cembran · J. Gao (✉)
Department of Chemistry, University of Minnesota,
Minneapolis, MN 55455, USA
e-mail: gao@chem.umn.edu

1 Introduction

Excited state intramolecular proton transfer (ESIPT) reactions are involved in numerous photochemical processes, including lasers [1], energy and data storage devices, optical switches [1–7], Raman filter [8], polymers photostabilizers [9], triplet quenchers [10,11], and LED materials [11]. These technological applications prompted extensive experimental [12–24] and theoretical [24–30] investigations. One model system that have been used is 1-acylamino-anthraquinones (AAQs) [20–24,29], a family of molecules that provide a framework for studying ESIPT reactions because of the rigidity of the backbone structure. Moreover, the chemical reactivity of these compounds can be conveniently modulated simply by changing the electron-withdrawing ability of the acyl substituent. Experimentally, it was observed that upon photoexcitation to the spectroscopic S_1 state, these chromophores can undergo ESIPT from the "normal" structure **N**, where the hydrogen is bonded to the nitrogen, to the tautomeric form **T**, in which the hydrogen is transferred to the oxygen (Fig. 1) [20]. We aim to model the dynamics of this ESIPT process by molecular dynamics simulations to understand solvation effects. In this article, we describe the construction and parameterization of the potential energy functions for the proton transfer reaction in the ground and excited states.

Early works [20–22] explored the photoreactivity of AAQs with spectroscopic methods, by probing the evolution of the energy gap between electronic states of the chromophore accompanying the ESIPT reaction. It was shown that the ESIPT process can be tuned by varying the substituent on the amino group. In particular, electron-withdrawing substituents show a fast (100 fs or less) and complete proton transfer (PT) after photoexcitation, whereas alkyl substituents tilt the equilibrium toward the **N** structure and hinder the PT. The

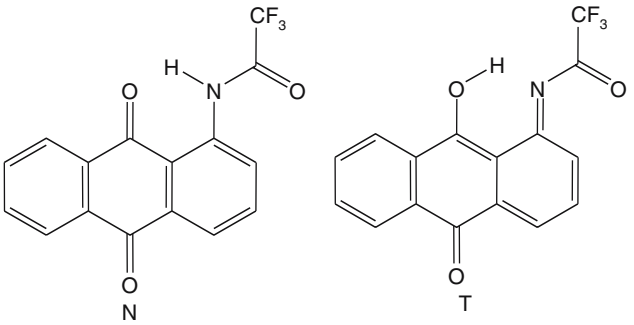

Fig. 1 Molecular structures of the normal (**N**) reactant state and the tautomer (**T**) product state of 1-(trifluoroacetylamino)anthraquinone (TFAQ)

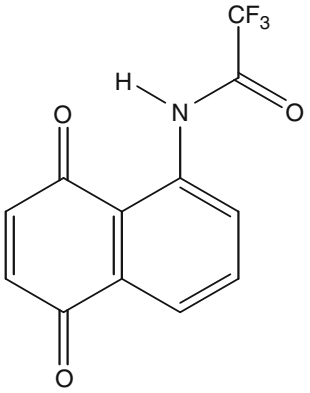

Fig. 2 1-(trifuloroacetylamino)naphtaquinone (TFNQ)

excited state lifetime of these molecules ranges from 80 to 700 ps and the decay to the ground state takes place by intersystem crossing.

Schmidtke et al. [23,24] recently applied a new Raman technique [31,32] that probed the solvent response to the ESIPT reactions of four AAQs in acetonitrile and dichloromethane solutions. This research provided further insights into the chromophore reactivity as well as solvent reorganization, the latter of which was found to play an important role in the reaction dynamics. In connection with the experimental work, we have previously investigated the intrinsic reactivity and free energy surface for the ESIPT reaction of a truncated model, 1-(trifuloroacetylamino)naphtaquinone (TFNQ), using high-level quantum mechanical (QM) methods (Fig. 2) [29]. Thus, the parent molecule, 1-(trifluoroacetylamino) anthraquinone (TFAQ), which has been found experimentally [20,23,24] to undergo ultrafast PT, was modeled by a smaller compound with the removal of the third aromatic ring from the antraquinone moiety to reduce the computational cost. We have shown that TFNQ is an adequate model compound for this system by comparison of the computed excitation energies with TFAQ. The main conclusions of the previous CASPT2//CASSCF investigations of TFNQ are summarized below, which are used in this work to parameterize an empirical model for condensed phase simulations.

In the ground state S_0, the proton is bonded to the nitrogen atom, which is the only minimum at the CASPT2 level of theory. A minimum structure was located for the proton transfer **T** state using CASSCF(10e,10o)/6-31G(d) optimization and CASSCF(12e,12o) energy calculation, but it is no longer a stationary state and the transition state S_0–TS that separates the two structures vanishes when dynamic correlations are included. The first excited state also has two minima at the CASSCF level, but as in the ground state, the PT reaction from the Franck–Condon (FC) region to the S_1–T structure is barrierless using the CASPT2 method. The computed excitation energy is 77.3 kcal mol^{-1}, which is in good accord with the experimental value 74.1 kcal mol^{-1}. The excited-state proton transfer is exothermic, releasing 14.2 kcal mol^{-1} at the CASPT2 level, and this energy can be partitioned into two contributions. The backbone relaxation from the spectroscopic FC state to the S_1 minimum (at the CASSCF level) is responsible for 11.7 kcal mol^{-1} and involves mainly "backbone" stretching modes with the proton transfer coordinate essentially unchanged, while 2.5 kcal mol^{-1} are due to the actual PT on the excited state surface. As will be shown later, after the initial geometry relaxation from the FC state, the PT surface is remarkably flat. Consequently, the proton is only weakly bonded to the oxygen in the excited state, which can undergo large oscillations along the reaction coordinate. While the magnitude and direction of the dipole moment of TFNQ are similar along the entire PT reaction coordinate in the ground state, photoexcitation to the FC region orients the dipole moment by about 90°, nearly perpendicular to that of the S_0 state. Interestingly, the dipole moment is realigned in the direction of the ground state as the proton is transferred to the oxygen site, with an increase in its magnitude by about 2 D.

The purpose of this work is to develop a molecular mechanics (MM) force field (FF) to describe the ESIPT for TFNQ and implement it into the CHARMM package [33]. This potential will be used in subsequent work to disentangle the contributing factors of the observed solvent dynamics accompanying the ESIPT [23,24]. Therefore, not only we aim to construct a reliable force field both for the ground and excited state of the isolated TFNQ molecule, but also we develop a potential function that can accurately describe its electrostatic properties and interactions with the solvent along the entire PT reactive coordinate. Our potential is a combination of the empirical valence bond (EVB) approach for the bonding terms, modeled to be applicable to both the ground and excited state [34,35], and a scheme to treat the electrostatic interactions by expressing the TFNQ atomic partial charges as a cubic spline function of the reaction coordinate. The reliability of the method is validated by computing the potential of mean force (PMF) for the PT in gas phase and in water solution.

In Sect. 2, we describe the theoretical model and simulation details. Then, the results and discussion will be presented in Sect. 3. We conclude this paper with a summary of the main findings of this work.

2 Methods

2.1 The EVB model

In order to study chemical reactions in the condensed phase, it is necessary to use a model that can adequately describe the breaking and forming of chemical bonds. Obviously, quantum mechanical method is an ideal choice, but it is still computationally intractable for large systems, especially when quantitative energetic results are of interest. Although combined QM/MM methods [35,36] may be used, it is rather complicated when the reaction of interest takes place on an electronically excited state. While several methods are being developed for this purpose [37–39], the semiempirical models [40] commonly used are parameterized for the ground state. Thus, it is necessary to carry out extensive parameterization for the excited state potential surfaces, and the work of Martinez is particularly notable [37,38].

In the present work, we decided to use the conventional approach by fitting empirical potential functions to reproduce the potential surfaces from ab initio calculations. Since we are primarily interested in the *adiabatic* reaction taking place either on the ground or the first excited state for the proton transfer reaction, it is adequate to employ semiempirical valence bond methods that have been used in similar applications [34,35]. In particular, we use one specific version of the semiempirical valence bond models, i.e., the empirical valence bond (EVB) terminology described by Warshel and Russel [34,35], in which the resonant structures of the reactant and product are represented by classical force fields, and the coupling is tuned to match the experimental or computational barrier height of the reaction. Here, we implement the EVB scheme to describe the PT potential surfaces both in the ground and the excited state for TFNQ. We note that Vendrell et al. [41] also successfully applied this approach to describe the excited state enol-keto photoisomerization for 2-(2′-hydroxyphenyl)-4-methyloxazole in gas phase and different solvents by parameterizing the potential to reproduce results from time-dependent density functional theory calculations.

Here, the Hamiltonian of Eq. 1 is calibrated to fit the results for the PT reaction both in the S_0 and in the S_1 state, and the target potential energy surfaces (PESs) are determined at the CASPT2//CASSCF level of theory [29]:

$$H(\mathbf{R}) = H_{\mathrm{EVB}}(\mathbf{r_H}, \mathbf{r_N}, \mathbf{r_O}) + H_{\mathrm{UB}}(\mathbf{r_N}, \mathbf{r_O}) + H_{\mathrm{CHARMM}}(\mathbf{R}) \quad (1)$$

where $\mathbf{R}$ represents the nuclear coordinates for all the atoms of TFNQ, and $\mathbf{r_H}$, $\mathbf{r_N}$, and $\mathbf{r_O}$ are, respectively, the coordinates for the hydrogen, nitrogen and oxygen atoms associated with the PT. $H_{\mathrm{EVB}}(\mathbf{r_H}, \mathbf{r_N}, \mathbf{r_O})$ is an EVB term (Eq. 2), fitted individually to represent either the ground or excited state:

$$H_{\mathrm{EVB}} = \varepsilon = \frac{(H_{11} + H_{22}) + \sqrt{(H_{11} - H_{22})^2 - 4H_{12}^2}}{2} \quad (2)$$

The two bonding terms in Eq. 2 are represented by a Morse potential [42];

$$H_{ii}(\mathbf{r_H}, \mathbf{r_N}, \mathbf{r_O}) = D_i(e^{-2\alpha_i(d_i - d_i^e)} - 2e^{-\alpha_i(d_i - d_i^e)}) \quad (3)$$

where d_i and d_i^e are respectively the proton bond distance and equilibrium bond distance (to $i = 1$ for the nitrogen and $i = 2$ for the oxygen). The off-diagonal term, $H_{12}(\mathbf{r_H}, \mathbf{r_N}, \mathbf{r_O}) = H_{21}(\mathbf{r_H}, \mathbf{r_N}, \mathbf{r_O})$, is approximated by an exponential function:

$$H_{12}(\mathbf{r_H}, \mathbf{r_N}, \mathbf{r_O}) = Ae^{-\mu(Rc(\mathbf{r_H}, \mathbf{r_N}, \mathbf{r_O}) - T)} \quad (4)$$

where $R_C(\mathbf{r_H}, \mathbf{r_N}, \mathbf{r_O})$ is the reaction coordinate, defined as the difference between the H–N (d_1) and H–O (d_2) bonds distances $d_1 - d_2$. The parameters A, μ and T control, respectively the size, width and equilibrium position, through which it is possible to yield a smooth surface for the barrier that otherwise would arise in a narrow crossing region.

In addition, a Urey–Bradley term is included in Eq. 1 to ensure that the correct N–O distance is maintained during the entire PT reaction:

$$H_{\mathrm{UB}}(\mathbf{r_N}, \mathbf{r_O}) = k_{\mathrm{UB}}(d_{\mathrm{NO}} - d_{\mathrm{NO}}^e)^2 \quad (5)$$

where k_{UB} is the Urey–Bradley force constant and d_{NO} and d_{NO}^e are respectively, the N–O bond distance and its equilibrium position. The last term in Eq. 1, $H_{\mathrm{CHARMM}}(\mathbf{R})$, includes the classical MM treatment for all the remaining energy terms describing TFNQ in the CHARMM27 force field [43,44].

The parameters in the EVB and Urey–Bradley terms are optimized by minimizing the scoring function in Eq. 6.:

$$S(\mathbf{R}) = \sum_{i=1}^{N} \sum_{j=1}^{M=7} w_j \left(\frac{Y_{i,j} - Y_{i,j}^{\mathrm{QM}}}{Y_{i,j}^{\mathrm{QM}}} \right)^2 \quad (6)$$

where the first summation is over molecular structures that have been considered, and the second sum runs over the seven target properties (i.e., relative energy, N–H and O–H bond distances, C–N–H and C–O–H bending angles, N–O Urey-Bradley distance and N–H–O angle). In Eq. 6, w_i is a weighting factor, $Y_{i,j}$ and $Y_{i,j}^{\mathrm{QM}}$ are the properties evaluated using the EVB model and the corresponding target values determined at the CASSCF level, respectively. There are three stationary structures optimized at the CASSCF level in the ground state S_0 (Fig. 5), which are the reacant N (S_0–N), the product T (S_0–T) and a transition structure (S_0–TS). For the excited state we have obtained a minimum relaxed in the vicinity

Table 1 Parameters in the empirical valence bond potential optimized for the S_0 and S_1 states

	Parameter	S_0	S_1
Morse 1	D_1(kcal mol^{-1})	350.0	300.0
	α_1 (Å^{-1})	1.00	1.25
	d_1^e (Å)	1.000	1.012
Morse 2	D_2 (kcal mol^{-1})	324.0	303.7
	α_2 (Å^{-1})	1.50	1.30
	d_2^e (Å)	0.970	0.977
H_{12}	A (kcal mol^{-1})	43.0	48.0
	μ (Å^{-1})	1.4	1.1
	T (Å)	0.08	0.01
Urey–Bradley	k_{UB} (kcal mol^{-1} Å^{-2})	210.0	2.7
	d_{NO}^e (Å)	300.0	2.7

of the FC region (S_1–N) and the PT product (S_1–T) as well as a transition structure on a very shallow potential surface. Although only S_0–N and S_1–T remain stationary structures at the CASPT2 level, we have used all structures determined using CASSCF to calibrate geometrical changes of TFNQ as a function of the PT reaction coordinate. Note that although the S_1–N structure is not a true minimum, it is still useful to calibrate the backbone structure relaxation immediately after photoexcitation, prior to proton transfer. The optimized parameters are listed Table 1.

2.2 The force field and molecular geometries

The EVB term in the Hamiltonian of Eq. 1 consists of two bond lengths associated with the transferring proton; the rest of the geometrical parameters are modeled by molecular mechanical force field, for which we adopt the standard formalism in the CHARMM27 force field [43,44]. For the ground state, we use the parameters of the CHARMM27 force field [43,44] for similar functional groups initially. To reproduce the target geometries of the S_0–N and S_1–T state, a number of bond stretching parameters were adjusted. We found that it was not required to modify the original values for the bending and torsional terms. Note that the stretching parameters are optimal for the minimum structure on each state, i.e., S_0–N and S_1–T, where the system spends most of the time: they are not a function of the reaction coordinate.

This simple adjustment works well for the S_0 state, but the excited state process involves an initial "backbone" structural relaxation from the FC state to a configuration prior to the actual proton transfer reaction, and this structural variation lowers the potential energy by 11.7 kcal mol^{-1} [29]. The proton transfer potential surface on the excited state, in fact, is rather flat, with an energy change of only 2.5 kcal mol^{-1} in favor of the S_1–T structure, which is included in the EVB model. The contribution of the backbone relaxation must be accounted for by adjusting the internal force field parameters. To this end, we have scaled the bond lengths and the corresponding force constants for those that exhibit large changes from the S_0–N to the S_1–T structure. Bending and torsion parameters have little alterations and are left unchanged. We used the scaling scheme adapted from reference [45], which is given below:

$$k_{ex} = k_{gr}\left(\frac{d_{gr}^e - 0.68}{d_{ex}^e - 0.68}\right)^3 \tag{7}$$

where d_{gr}^e and d_{ex}^e are, respectively, the S_0–N and S_1–T equilibrium bond distances, and k_{gr} and k_{ex} are the stretching force constants.

The overall rescaling procedure leads to a relaxed S_1–T structure in reasonable agreement with that optimized at the CASSCF level, and the energy change also matches the ab initio result. The complete set of bonding parameters used for both states which can be directly used in the CHARMM program is provided in the supporting information in Table S1.

2.3 Nonbonded terms and solute–solvent bimolecular complexes

Nonbonded interactions are described by a combination of Lennard–Jones and Coulombic terms. Initially, the van der Waals parameters are taken from the CHARMM27 force field [43,44] for atoms of similar types, whereas the parameters for fluorine and for the fluorinated carbon are taken from reference [46]. However, we have reduced the value of the energy depth by one half in view of the work described in reference [47]. These are further refined by considering bimolecular molecular interactions (see below).

Previously, [29] we have determined the atomic partial charges of TFNQ for structures both in the ground and the excited state by fitting the electro-static potentials [48] (ESP) computed using CASSCF(12,12)/6-31G(d). To smoothly describe the change in electrostatic properties of TFNQ as a function of the PT reaction coordinate, the ESP atomic charges are then interpolated with a cubic spline function [49] along the reaction coordinate in the interval from –1.5 to +1.5Å. In particular, the S_0–N, S_0–TS and S_0–T structures for the ground state and the S_0–N, S_1–N, S_1–TS and S_1–T structures for the excited state, all from CASSCF optimizations, are used to obtained partial charges at various solute geometries. However, to adequately describe solute-solvent interactions both in the ground and in the excited state, it is not sufficient to simply adopt the ESP charges. To this end, we have further adjusted these partial charges by considering TFNQ and water bimolecular complexes. This is particularly

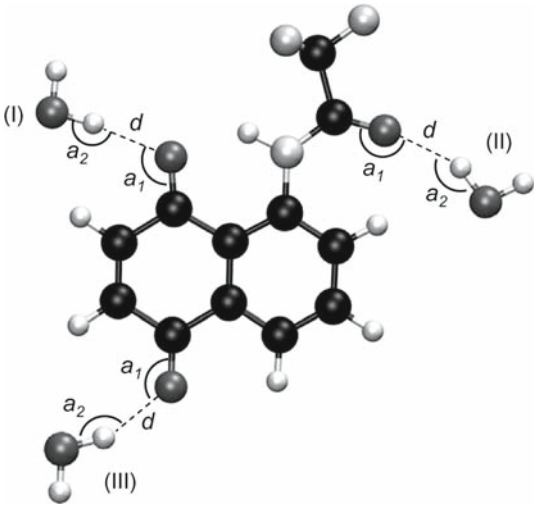

Fig. 3 Schematic illustration of the TFNQ-H_2O bimolecular complexes in three different binding sites. Notice that each bimolecular complex is optimized separately at the HF/6-31G(d) level of theory or by using the empirical valence bond potential

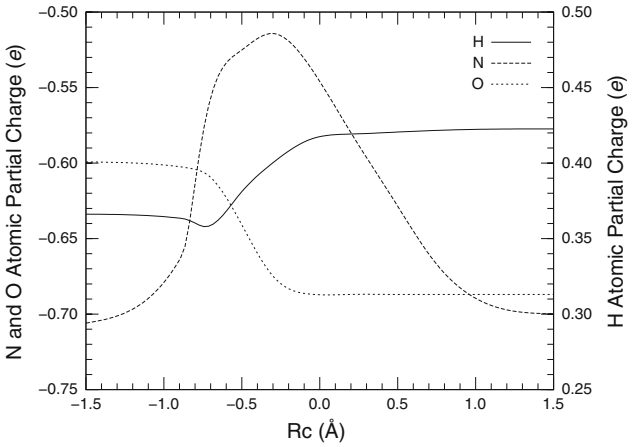

Fig. 4 Variation of partial atomic charges in the excited state, depicted by a cubic spline function along the proton transfer reaction coordinate. The donor (*N*), the acceptor (*O*) and the proton (*H*) directly associated with the proton transfer reaction are illustrated. Note the different scales for O and N (*left*) and H (*right*). All atomic charges are given in electron units

Table 2 Computed dipole moments and orientations relative to that of the ground state minimum S_0–N for the model compound TFNQ in the gas phase

		Spline charge model		CASSCF/6-31G(d) [29]	
		$\|\mu\|$ (Debye)	θ (Degrees)	$\|\mu\|$ (Debye)	θ (Degrees)
S_0	S_0–N	2.63	0	2.64	0
	S_0–TS	2.77	13	2.82	8
	S_0–T	1.38	37	1.42	29
S_1	S_0–N	1.41	90	1.63	94
	S_1–N	1.93	116	2.58	115
	S_1–TS	2.09	100	2.81	99
	S_1–T	4.79	12	4.54	2

Table 3 Computed binding energies and geometrical parameters for TFNQ-water bimolecular complexes in the ground state

Complex		HF/6-31G*	MM
(I)	$-\Delta E$	5.23	4.87
	d	2.13	1.99
	a_1	121	125
	a_2	149	160
(II)	$-\Delta E$	4.95	4.57
	d	2.12	2.08
	a_1	166	165
	a_2	150	161
(III)	$-\Delta E$	5.62	5.21
	d	2.10	1.98
	a_1	123	120
	a_2	149	161

Structures are depicted in Fig. 3. The results obtained by using the present empirical potential are compared with those obtained at the HF/6-31G* level. Energies are given in kcal mol^{-1}, distances in Angstroms and angles in degrees

important in view of the flat potential surface for the PT on the excited state, suggesting that specific solute-solvent interactions can modulate the proton transfer rate.

Both atomic partial charges and van der Waals parameters, in particular, for atoms participating in hydrogen bond interactions, are readjusted from the initial values. We have determined the binding energies and geometries associated with hydrogen bonding interactions for three TFNQ-H_2O complexes on the ground state (Fig. 3) at the HF/6-31G* level, in which the monomer geometries are held fixed. The same clusters are then minimized using the present force field along with the water model developed by Skinner and coworkers [50]. Table 2 compares the computed dipole moments and relative orientations to the ground state minimum determined using the final set of charges, represented by a spline function along the reaction coordinate, with those obtained from the original QM model. Overall, the agreement is excellent both in dipole magnitude and in orientation in ground and excited states. Figure 4 illustrates the atomic charge variations on the S_1 surface along the reaction coordinate for the donor, acceptor and the transfer proton atoms. Finally, the computed binding interaction energies and hydrogen bonding geometries using the present empirical potential are given in Table 3, which are compared with the results determined by full QM calculations. All parameters for TFNQ are given in the supporting information.

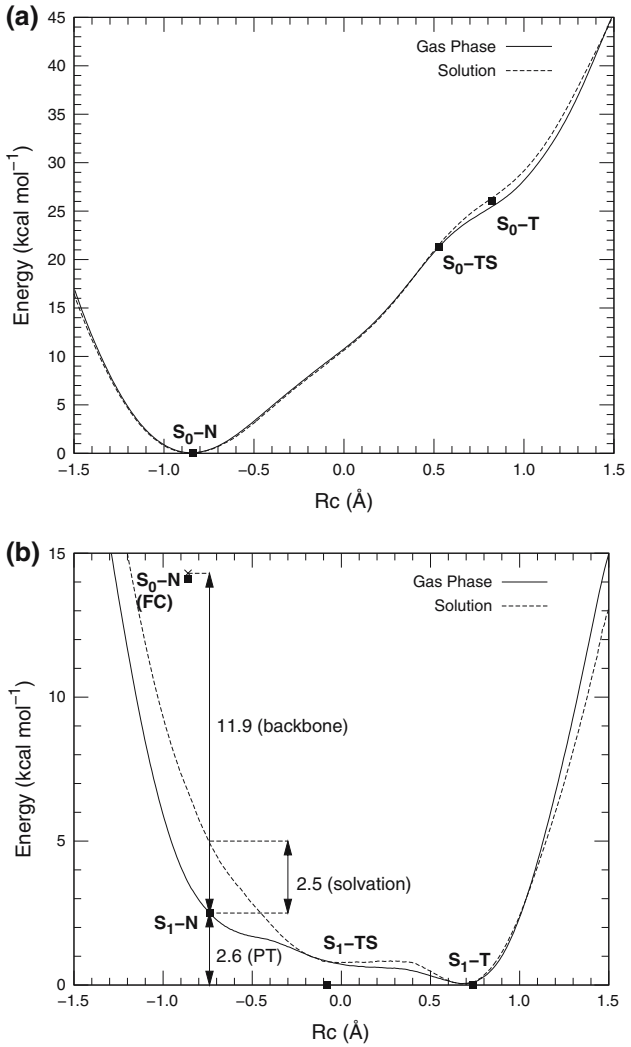

Fig. 5 Computed potential of mean force (PMF) for the ground state (**a**) and for the excited state (**b**) of TFNQ in the proton transfer reaction in the gas phase (*solid line*) and in aqueous solution (*dotted line*). The cross marks indicate relative energies determined at the CASPT2 level of theory. The Franck–Condon energy for the S_0–N structure computed using the present empirical potential for the S_1 state is indicated by a *circle* in (**b**). Note that about 12 kcal mol^{-1} of energy is released from the FC state without substantial displacement along the reaction coordinate, whereas the PT contributes about 2.5 kcal mol^{-1} to the overall energy change. The solvation effect (2.6 kcal mol^{-1}) is also highlighted for the S_1–N structure

In the present model, nonbonded interactions within the solute TFNQ are excluded, i.e., the solute atoms only interact with the solvent. This approach is justified by the fact that the only atom that can significantly move within the molecule, the transferred proton, is specifically treated by the EVB approach, parameterized to reproduce the QM potential surface. Since the solute molecule is rather small and relatively rigid, the internal force field terms are sufficient to describe the motions of other atoms in the molecule.

The dependency of the partial charge on the reaction coordinate Rc is reflected in the pair interactions between the solute TFNQ and solvent m, U_m:

$$U_m[\mathbf{r}_s, \mathbf{r}_m, \mathrm{Rc}(\mathbf{r_H}, \mathbf{r_N}, \mathbf{r_O})] = \frac{1}{4\pi\varepsilon_0} \sum_{i=1}^{\text{solute}} \sum_{j=1}^{\text{solvent}} \frac{q_i\,[Rc(\mathbf{r_H}, \mathbf{r_N}, \mathbf{r_O})]\,q_j}{r_{ij}} \tag{8}$$

The subscript "s" refers to the solute molecule, r_{ij} is the distance between atom i of the solute and atom j of the solvent, and $q_i[\mathrm{Rc}(\mathbf{r_H}, \mathbf{r_N}, \mathbf{r_O})]$ emphasizes that the solute atomic charges is dependent on the reaction coordinate. Thus, when evaluating forces, the terms dependent on the reaction coordinate must be included.

2.4 Simulation details

The potential of mean force (PMF) for the proton transfer reaction both in the gas phase and in water, in the two electronic states, have been determined to examine the performance of the potential energy surface. We used the umbrella sampling [51] technique coupled with the weighted histogram analysis method [52] to span a range from –1.5 to 1.5 Å in the proton transfer coordinate, which is defined as the difference between the proton from the donor and acceptor distances. In all, a total of 31 and 15 simulations (also called windows) have been used for the gas phase and solution phase simulations, respectively.

For the simulations in aqueous solution, one solute molecule is immersed in a cubic box of roughly $36 \times 36 \times 36$ Å^3, consisting of 1,522 water molecules. The water model is the flexible four-site potential developed by Lawrence and Skinner [50], which provides an excellent treatment of the vibrational spectrum of liquid water. Periodic boundary conditions are used along with the isothermal-isobaric ensemble at 298 K and 1 atm, controlled by the Nosé–Hoover thermostat [53,54]. Group-based nonbonded interactions are truncated with a switching function between 14 and 15 Å. We used the leap-frog integration algorithm [55] with a time-step of 0.5 fs to propagate the equations of motion. For each window, an equilibration lasting 100 ps is followed by additional 100 ps for statistical averaging. For the gas phase calculations, each window involves 10 ps of equilibration, followed by 100 ps of sampling.

3 Results and discussion

3.1 Potential of mean force in the gas phase

The ground and excited states PMFs computed in gas phase are reported in solid lines in Fig. 5. The agreement with the relative energies for the structures computed at the QM level

[29] (black squares) is excellent. The only small difference between the CASPT2 value and the PMF result is at the excited state transition state structure optimized at the CASSCF level of theory, where the value obtained from the force field simulations is 0.7 kcal mol^{-1} higher than the ab initio data. This is due to the intrinsic difficulty in reproducing the extended flat region between S_1–TS and S_1–T by using the EVB formalism. The QM calculations also showed that there is no barrier on the excited state for the PT reaction: by carefully tuning the EVB parameters, and in particular the off-diagonal coupling term, we are able to reproduce the same feature.

It is worth to notice that the energy partition into contributions from backbone structural relaxation and proton transfer reaction noted above is also reproduced. We notice in Fig. 5b that the PT is responsible for 2.6 kcal mol^{-1} of energy release, while the backbone relaxation from the FC region contributes additional 11.9 kcal mol^{-1} to the overall exothermicity.

3.2 Potential of mean force in water

The PMFs computed for the ground and excited state in aqueous solution are depicted in dotted lines in Fig. 5. First, there is little solvent effects on the ground state potential of mean force by aqueous salvation (Fig. 5a) and the computed PMF in the gas phase nearly coincides that in water, consistent with the small changes in molecular dipole moment along the PT pathway. Furthermore, the changes in hydrogen bonding energy for bimolecular complexes are relatively small (Table 3).

On the other hand, the change in dipole moment up on photoexcitation is rather dramatic, which increases by 2 Debye with an initial reorientation of the solute dipole perpendicular to the ground state at the FC region, followed by relaxation to the same direction at the product side. Schmidtke et al. [24] found that the **T** state is stabilized by about 1 kcal mol^{-1} in acetonitrile and by 0.7 kcal mol^{-1} in dichloromethane compared to the gas phase profile. Figure 5b shows that aqueous salvation provides even greater stabilization of the S_1–T product state than the structure near the ground state minimum (relaxed FC state, S_1–N). In comparison with the gas phase PMF, the free energy in the region spanning from S_1–TS to the S_1–T product state is lowered by about 2.5 kcal mol^{-1} relative to S_1–N. Table 2 shows that the S_1–TS structure has similar dipole moment as that of the S_1–N structure, whereas it is much greater in the S_1–T state. Since the stabilizing effects are similar to the S_1–TS and S_1–T states despite the fact that they have quite different dipole moments, the results suggest that there is compensating balance effects of solvent dynamics and entropic contributions as a result of dipolar re-orientation during the proton transfer process. These questions will be addressed in a future paper on dynamic trajectory investigations of the excited state proton transfer process.

In Table 3, we report the sum of interaction energies of the three TFNQ-water bimolecular complexes, which happens to be about 2.5 kcal mol^{-1} stabilizing S_1–T relative to S_1–N. On the other hand, the difference in the clusters energies between S_1–T and S_1–TS is only 0.8 kcal mol^{-1}. Thus, careful consideration of the detailed specific hydrogen bonding interactions is important in developing potential energy functions, and these effects are not always reflected by the magnitude of molecular dipole moment.

4 Conclusions

In this study, we describe a molecular mechanics force field for the study of the excited state intramolecular proton transfer reaction in the TFNQ. We implemented the empirical valence bond technique to describe the chemical process both in the ground and the first excited state. To model the continuous charge variation along the proton transfer reaction pathway, we used a cubic spline function to represent the partial atomic charges. Nonbonded parameters are fitted to reproduce molecular dipole moments computed at the CASSCF level of theory and to reproduce ab initio hydrogen bonding energies and geometries for TFNQ-water bimolecular complexes. The utility of this potential energy function was examined by computing the potentials of mean force for the proton transfer reactions in the gas phase and in water, in both electronic states. The ground state PMF exhibits little solvent effects, whereas computed potential of mean force shows a solvent stabilization of 2.5 kcal mol^{-1} in the product state region, suggesting proton transfer is more pronounced in polar solvents, consistent with experimental findings. We are currently applying the present potential to investigate the solvent dynamical response to the ESIPT reaction.

Acknowledgments The work was partially supported by the Minnesota Supercomputing Institute through a Scholarship to A.C. and by the Army Research Laboratory through the Arm High-Performance Computing Research Center (AHPCRC) under the auspices of the Department of the Army, Army Research Laboratory DAAD 19-01-2-0014. We thank Professor David Blank for discussion.

References

1. Chou PT, McMorrow D, Aartsma TJ, Kasha M (1984) J Phys Chem 88:4596
2. Ernsting NP, Nikolaus B (1986) Appl Phys B-Lasers Opt 39:155
3. Ferrer ML, Acuna AU, Amatguerri F, Costela A, Figuera JM, Florido F, Sastre R (1994) Appl Optics 33:2266
4. Jones G, Rahman MA (1994) J Phys Chem 98:13028
5. Liphardt M, Goonesekera A, Jones BE, Ducharme S, Takacs JM, Zhang L (1994) Science 263:367
6. Douhal A, Sastre R (1994) Chem Phys Lett 219:91

7. Kuldova K, Corval A, Trommsdorff HP, Lehn JM (1997) J Phys Chem A 101:6850
8. Martinez ML, Cooper WC, Chou PT (1992) Chem Phys Lett 193:151
9. Heller HJ, Blattmann HR (1973) Pure Appl Chem 36:141
10. Werner T (1979) J Phys Chem 83:320
11. Tarkka RM, Chen XL, Jenekhe SA (1997) In: Jenekhe SA, Wynne KJ (ed) Photonic and optoelectronic polymers (Acs Symposium Series), vol 672. American Chemical Society, Washington DC. pp 475
12. Weller A (1955) Naturwissenschaften 42:175
13. Sengupta PK, Kasha M (1979) Chem Phys Lett 68:382
14. Elsaesser T, Kaiser W, Lüttke W (1986) J Phys Chem 90:2901
15. Ormson SM, Brown RG (1994) Progress in reaction kinetics 19:45
16. Legourrierec D, Ormson SM, Brown RG (1994) Progress in reaction kinetics 19:211
17. Mitchell P (1961) Nature 191:144
18. Arnaut LG, Formosinho SJ (1993) J Photo Chem Photobiol. A 75:1
19. Neuwahl FVR, Foggi P, Brown RG (2000) Chem Phys Lett 319:157
20. Smith TP, Zaklika KA, Thakur K, Walker GC, Tominaga K, Barbara PF (1991) J Phys Chem 95:10465
21. Neuwahl FVR, Bussotti L, Righini R, Buntinx G (2001) Phys Chem Chem Phys 3:1277
22. Srivatsavoy VJP, Venkataraman B (1990) Chem Phys Lett 174:406
23. Schmidtke SJ, Underwood DF, Blank DA (2004) J Am Chem Soc 126:8620
24. Schmidtke SJ, Underwood DF, Blank DA (2005) J Phys Chem A 109:7033
25. Mitra S, Das R, Bhattacharyya SP, Mukherjee S (1997) J Phys Chem A 101:293
26. Moller S, Andersen KB, Spanget-Larsen J, Waluk J (1998) Chem Phys Lett 291:51
27. Prieto FR, Rodriguez MCR, Gonzalez MM, Fernandez MAR (1994) J Phys Chem 98:8666
28. Maheshwari S, Chowdhury A, Sathyamurthy N, Mishra H, Tripathi HB, Panda M, Chandrasekhar J (1999) J Phys Chem A 103:6257
29. Cembran A, Gao J (2006) Mol Phys 104:943
30. Scheiner S (2000) J Phys Chem A 104:5898
31. Underwood DF, Blank DA (2003) J Phys Chem A 107:956
32. Underwood DF, Blank DA (2005) J Phys Chem A 109:3295
33. Brooks BR, Bruccoleri RE, Olafson BD, States DJ, Swaminathan S, Karplus M (1983) J Comput Chem 4:187
34. Warshel A (1991) Computer modeling of chemical reactions in enzymes and solutions. Wiley, New York
35. Aaqvist J, Warshel A (1993) Chem Rev 93:2523
36. Gao J, Thompson MA (eds) (1998) Combined quantum mechanical and molecular mechanical methods. American Chemical Society, Washington, DC
37. Ben-Nun M, Martinez TJ (2002) Adv Chem Phys 121:439
38. Ben-Nun M, Quenneville J, Martinez TJ (2000) J Phys Chem A 104:5161
39. Bearpark MJ, Boggio-Pasqua M, Robb MA, Ogliaro F (2006) Theor Chem Acc 116:670
40. Pople JA, Santry DP, Segal GA (1965) J Chem Phys 43:S129
41. Vendrell O, Moreno M, Lluch JM, Hammes-Schiffer S (2004) J Phys Chem B 108:6616
42. Morse PM (1929) Phys Rev 34:57
43. MacKerell AD Jr., Bashford D, Bellott M, Dunbrack RL, Evanseck JD, Field MJ, Fischer S, Gao J, Guo H, Ha S, Joseph-McCarthy D, Kuchnir L, Kuczera K, Lau FTK, Mattos C, Michnick S, Ngo T, Nguyen DT, Prodhom B, Reiher WE, III, Roux B, Schlenkrich M, Smith JC, Stote R, Straub J, Watanabe M, Wiorkiewicz-Kuczera J, Yin D, Karplus M (1998) J Phys Chem B 102:3586
44. MacKerell AD Jr, Feig M, Brooks CL III (2004) J Comput Chem 25:1400
45. Pauling LC (1960) The nature of the chemical bond and the structure of molecules and crystals. An introduction to modern structural chemistry. 3rd ed. Cornell University Press, Ithaca
46. Chen IJ, Yin D, Mackerell AD Jr. (2002) J Comput Chem 23:199
47. Watkins EK, Jorgensen WL (2001) J Phys Chem A 105:4118
48. Cox SR, Williams DE (1981) J Comput Chem 2:304
49. Press WH, Teukolsky SA, Vetterling WT, Flannery BP (1994) Numerical recipes in fortran the art of scientific computing. Cambridge University Press, New York
50. Lawrence CP, Skinner JL (2003) Chem Phys Lett 372:842
51. Torrie GM, Valleau JP (1977) J Comput Phys 23:187
52. Kumar S, Bouzida D, Swendsen RH, Kollman PA, Rosenberg JM (1992) J Comput Chem 13:1011
53. Nose S (1984) J Chem Phys 81:511
54. Hoover WG (1985) Phys Rev. A 31:1695
55. Hockney RW (1970) In: Methods in computational physics, vol 9. Academic, New York, pp 136